Automated measurement of pulmonary artery in low-dose non-contrast chest CT images

Yiting Xie[a], Mingzhu Liang[b], David F. Yankelevitz[b], Claudia I. Henschke[b] and Anthony P. Reeves[a]

[a]School of Electrical and Computer Engineering, Cornell University, Ithaca, NY, USA
[b]Department of Radiology, Icahn School of Medicine at Mount Sinai, New York, NY, USA

ABSTRACT

A new measurement of the pulmonary artery diameter is obtained where the artery may be robustly segmented between the heart and the artery bifurcation. An automated algorithm is presented that can make this pulmonary artery measurement in low-dose non-contrast chest CT images. The algorithm uses a cylinder matching method following geometric constraints obtained from other adjacent organs that have been previously segmented. This new measurement and the related ratio of pulmonary artery to aortic artery measurement are compared to traditional manual approaches for pulmonary artery characterization.

The algorithm was qualitatively evaluated on 124 low-dose and 223 standard-dose non-contrast chest CT scans from two public datasets; 324 out of the 347 cases had good segmentations and in the other 23 cases there was significant boundary inaccuracy. For quantitative evaluation, the comparison was to manually marked pulmonary artery boundary in an axial slice in 45 cases; the resulting average Dice Similarity Coefficient was 0.88 (max 0.95, min 0.74). For the 45 cases with manual markings, the correlation between the automated pulmonary artery to ascending aorta diameter ratio and manual ratio at pulmonary artery bifurcation level was 0.81. Using Bland-Altman analysis, the mean difference of the two ratios was 0.03 and the limits of agreement was (-0.12, 0.18). This automated measurement may have utility as an alternative to the conventional manual measurement of pulmonary artery diameter at the bifurcation level especially in the context of noisy low-dose CT images.

Keywords: Pulmonary artery, low-dose CT, computer-based segmentation, pulmonary artery trunk measurement, ascending aorta measurement.

1. INTRODUCTION

The diameter of the pulmonary artery has been associated with several health risks[1-4]. Edwards et al[1] showed that an enlarged pulmonary artery was associated with hypertension. Devaraj et al[3] stated that the ratio of pulmonary artery diameter to ascending aorta diameter was moderately correlated with mean pulmonary arterial pressure. The conventional measurement of main pulmonary artery diameter in CT images is usually performed manually in an axial slice at the level of its bifurcation[1-4]. Automated and semi-automated methods to measure pulmonary artery diameter have been developed for cardiac CT and CTA images[5, 6].

In this study the pulmonary artery was segmented and measured in the axial plane between the heart and the pulmonary artery bifurcation, automatically, in low-dose non-contrast chest CT images. Due to the presence of high levels of noise in low-dose images, the main pulmonary artery at the level of the bifurcation does not always have a well-defined shape. Therefore measurement of pulmonary artery was conducted between the heart and the bifurcation, where it is more easily robustly segmented. The segmentation method employs both the intensity image and a pre-computed anatomy label map (ALM) containing region labels including the aorta, fatty tissues, lungs and the bony structures. The segmentation outcome was evaluated both visually and quantitatively compared to manual boundaries. The ratio of pulmonary artery diameter to ascending aorta diameter was also computed automatically.

2. METHODS

The algorithm segments the pulmonary artery between the heart and its bifurcation. Figure 1 shows an example of our segmentation target region as well as the main pulmonary artery at the bifurcation, which is commonly used in the literature[1-4] for manual measurement. The automated algorithm consists of two main steps: (1) Locate a set of slices that contain the pulmonary artery; then search for a seed point inside its lumen in each slice; (2) Fit a 3rd order polynomial function to the seed points to form a centerline; cast rays perpendicular to the centerline towards the pulmonary artery surface based on a triangular mesh model. A ray is terminated on a surface location if pre-defined conditions are satisfied. The detected surface points are mapped back to the original image to obtain the final segmentation region.
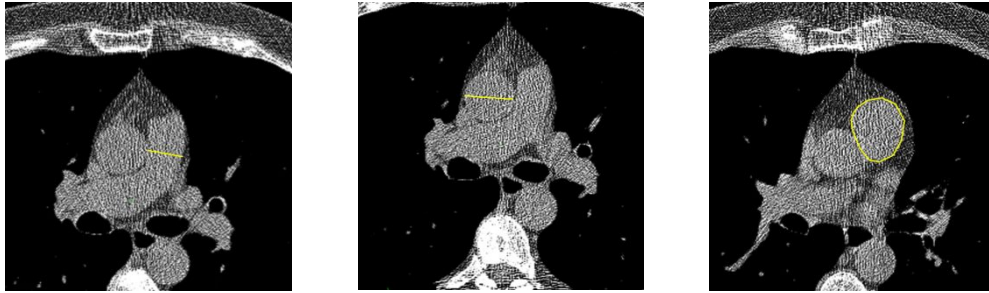

Figure 1 Measurement of pulmonary artery and ascending aorta at different locations: left image shows the manual measurement of diameter at the level of the bifurcation indicated by the yellow line; middle image shows the manual measurement of ascending aorta diameter in the same slice at the bifurcation level; right image shows our segmentation target between the heart and the bifurcation indicated by the yellow circle.

2.1 Detection of pulmonary artery seed points

Detection of pulmonary artery seed points is performed in an Anatomy Label Map where pre-segmented organs are labeled uniquely (see Figure 2). The set of slices in the space below the aortic arch and above the heart top is extracted[7]. The algorithm searches the unlabeled region in each slice on the left anterior side of the ascending aorta and fits a fixed sized circle (radius 10mm) in this region. A gravity constraint is imposed so that the circle will be close to the anterior region and the left lung. Figure 2 shows the seed point circles and the estimated centerlines (seed points) in 2 different cases. Note that the estimated seed points are not necessarily the center of the pulmonary artery. It is sufficient to be inside the pulmonary artery lumen.

2.2 Surface detection

After constraining the general location of the pulmonary artery, the following method is used to determine the actual surface location[8].

(1) A 3rd order polynomial function is fit to the seed points to obtain a centerline. A triangular mesh model is mapped to the polynomial centerline (Figure 3 (a) and (b)).
(2) Rays are projected perpendicular to the centerline towards the surface through the center of each triangle and intensity values along the ray are sampled (Figure 3 (b) and (c)).
(3) The intensity values for each ray are averaged with its 12 neighbors to reduce the effect of image noise, i.e.

$$\overline{S} = \frac{S + N_1 + ... + N_{12}}{13}$$ (Figure 3 (c)).

(4) The location of the intersection of each ray and the boundary of the artery is determined. For $\overline{S} = \{s_1, s_2, ..., s_m\}$, the intersection point is determined to be s_i, where $s_1, s_2, ..., s_{i-1}$ are unlabeled in the label map and s_i is either labeled or has an intensity in the range of fatty tissues.
(5) The measured surface points ($s_i, n_{1i}, n_{2i}, ...$) at the center of each triangle are used to determine the vertices' locations in the triangular mesh model, i.e. vertex $V = \frac{s_i + n_{1i} + ... + n_{7i}}{6}$. The triangular mesh model is then mapped back to the original image to determine the final segmentation (Figure 3 (c) and (d)).

(a)   (b)

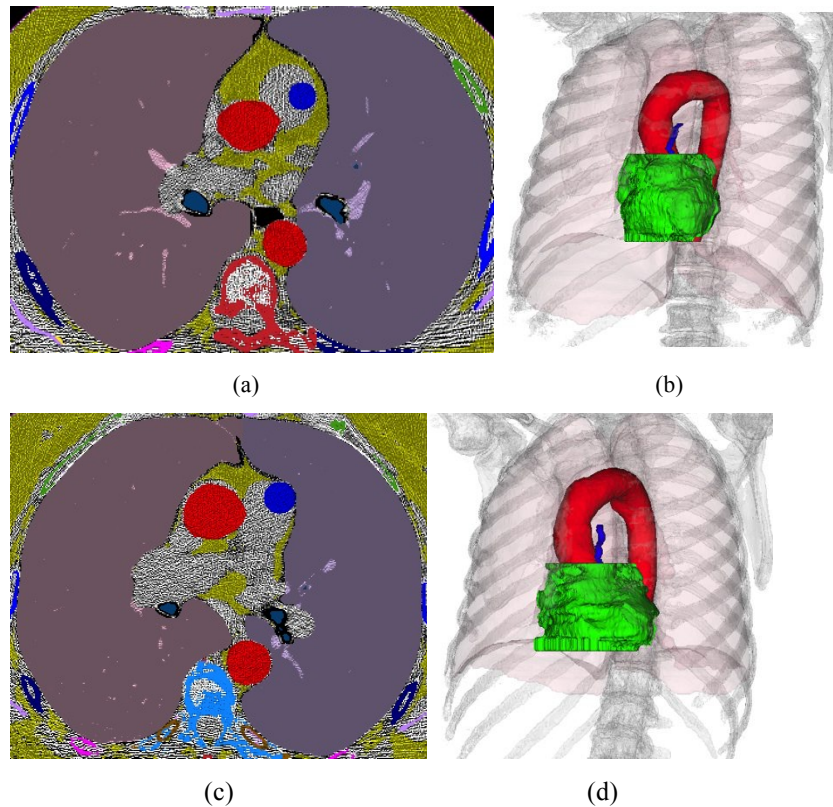(c)   (d)

Figure 2 Two examples showing seed point detection ((a), (b) belong to the first case and (c), (d) belong to the second case). Pre-segmented organs are overlaid on the intensity image in different colors in (a) and (c): aorta in red; lungs in purple; fatty tissues in yellow while the unlabeled region is in grey. The circles indicating seed points are in blue. They are located inside pulmonary artery lumen. In (b) and (d), the seed points (circle centers) are shown as the thin blue line.

Figure 4 shows the segmented pulmonary artery for two cases in axial slices as well in 3D image space. After segmentation of the pulmonary artery, the average pulmonary artery diameter is measured based on the area covered by the triangular mesh using the following method. The diameter of the pre-segmented ascending aorta is also computed[8].

(1) For each set of triangles on the same level perpendicular to the centerline, compute the total area covered by the triangles A_i and the equivalent diameter $D_i = 2\sqrt{\dfrac{A_i}{\pi}}$.

(2) The average diameter of the entire pulmonary artery region is the average of all the D_i in the triangular mesh model.

(a)   (b)

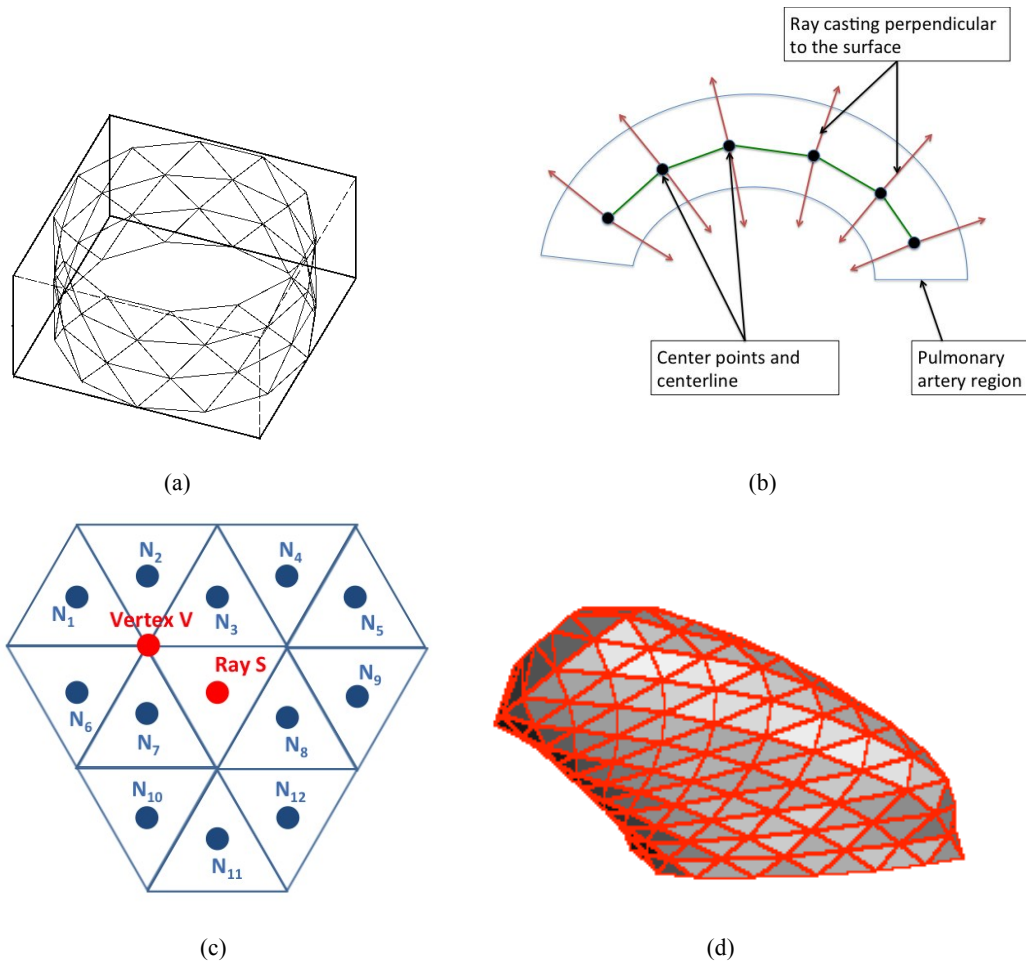(c)   (d)

Figure 3 Triangular mesh model for surface detection. Left image shows a triangular mesh with unit diameter and right image shows a triangular mesh representing the detected pulmonary artery surface.

3. EXPERIMENTS

Two experiments were conducted: the first experiment evaluated the segmentation quality both visually and quantitatively compared to manual boundaries; the second experiment studied the relationship between the automatically computed pulmonary artery to ascending aorta diameter ratio and the diameter ratio obtained from manual markings at the bifurcation level.

3.1 Dataset

Two public datasets with 347 images in total were used for evaluation. The first is the VIA-ELCAP public dataset[9] and contains 50 low-dose chest CT scans, among which 5 cases were excluded due to serious implant artifacts. The second dataset is the LIDC public dataset[10], which contains 335 low-dose and standard-dose non-contrast CT images, among which 33 cases were excluded due to serious implants artifacts, patient prone positions, abnormal anatomical structures or excessive image noise. In total 45 low-dose scans were used from VIA-ELCAP; 79 low-dose and 223 standard-dose chest CT scans were used from LIDC. All scan images are non-contrast.

Manual markings were performed for the 45 low-dose scans from VIA-ELCAP dataset at three different locations: main pulmonary artery diameter at the bifurcation level which is usually used in the literature for manual measurement of pulmonary artery (see Figure 1 left image); ascending aorta diameter at the bifurcation level (same slice as first marking, see Figure 1 middle image); pulmonary artery boundary in an axial slice (see Figure 1 right image), which is the middle slice in the segmented pulmonary artery region.
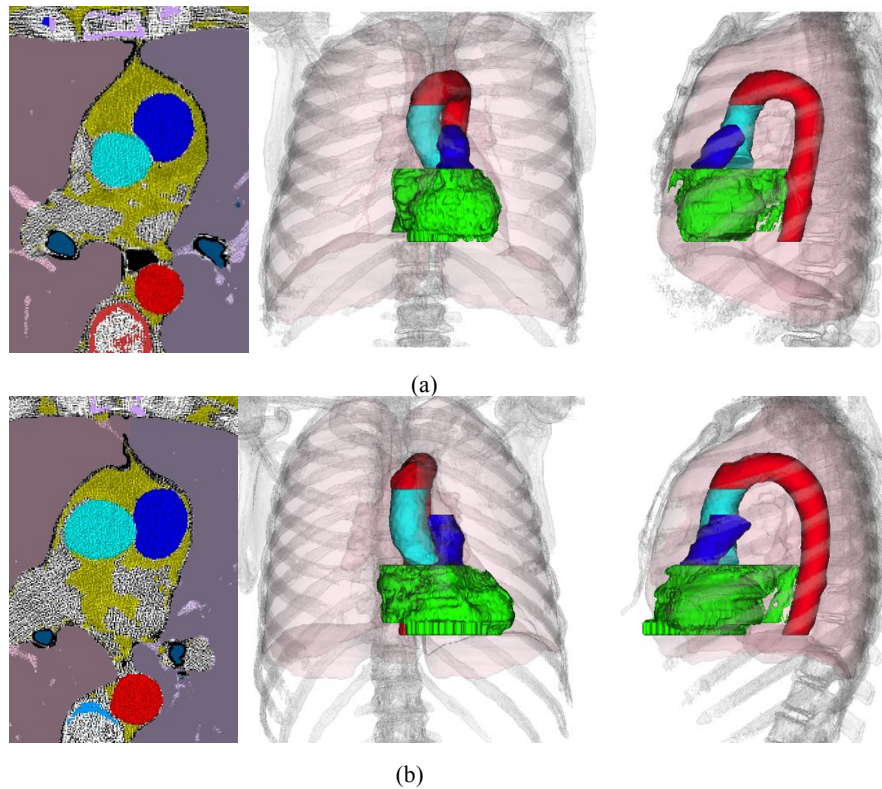
(a)

(b)

Figure 4 Segmented pulmonary artery for two cases ((a) and (b)) in axial, coronary and sagittal views. Pulmonary artery is in dark blue, ascending aorta in light blue, other aorta region in red and lung region in pink.

3.2 Experiments

Three experiments were performed for evaluation. The first experiment inspected the segmented pulmonary artery region visually by overlaying it on the intensity images for all evaluation cases. Segmentation without significant boundary inaccuracy was considered as good. The second experiment compared the automated segmentation with the manually marked boundary in the axial slice for the 45 VIA-ELCAP cases and the Dice Similarity Coefficient (DSC) was computed. The DSC is defined as twice the intersection between the automated and manual areas divided by the sum of the two areas. The third experiment compared the artery ratio outcomes for the manual and automated methods on the 45 cases with manual markings. In this experiment, the correlation between methods was reported and a Bland-Altman analysis was also performed to establish the limits of agreement.

4. RESULTS

For visual inspection, 324 out of 347 cases had good segmentation results while the other 23 cases had significant boundary inaccuracy in regions adjacent to other soft tissues. For quantitative evaluation using 45 low-dose scans, the automated algorithm had an average DSC of 0.88 (max 0.95, min 0.74). Figure 5 shows four cases comparing the automated region with the manual region.

Case1 DSC = 0.94

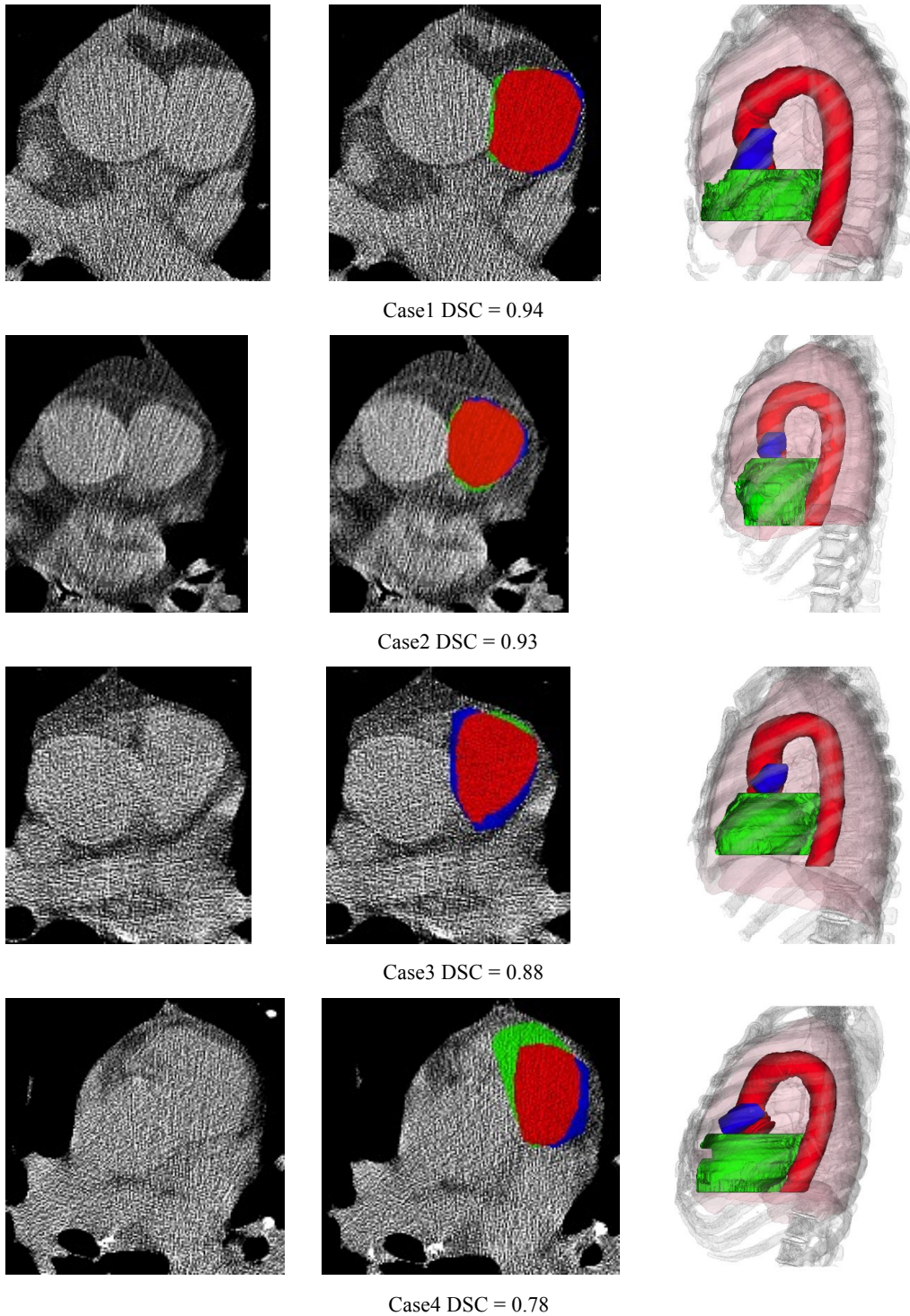Case2 DSC = 0.93

Case3 DSC = 0.88

Case4 DSC = 0.78

Figure 5 Pulmonary artery segmentation results from 4 example cases. In each row from left to right are: original image, segmented pulmonary artery in an axial slice and in 3D sagittal view. For the axial view: red is the overlapping region between automated and manual segmentation; green only exists in automated segmentation and blue only exists in manual segmentation. For the 3D sagittal view, red is the automated segmented aorta and blue is the automated segmented pulmonary artery.

For the 45 cases with manual markings, the results are summarized as follows:

- For the pulmonary artery measurements, the manual diameter had a mean of 25.96mm (max 35.01mm, min 19.16mm) and the automated diameter measurements had a mean of 26.56mm (max 34.26mm, min 20.99mm); their correlation (R^2) was 0.80 (see Figure 6(a));
- For the ascending aorta measurements, the manual diameter had a mean of 33.84mm (max 44.35mm, min 22.90mm) and the automated diameter had a mean of 33.31mm (max 39.96mm, min 23.81mm); their correlation was 0.93 (see Figure 6 (b));
- For pulmonary artery to ascending aorta diameter ratio, the manual ratio had a mean of 0.77 (max 1.10, min 0.53) and the automated ratio had a mean of 0.80 (max 1.17, min 0.60); their correlation was 0.81 (see Figure 7 (a)). Using Bland-Altman analysis, the mean difference was 0.03 and the limits of agreement (LOA) were (-0.12, 0.18) (see Figure 7(b)).
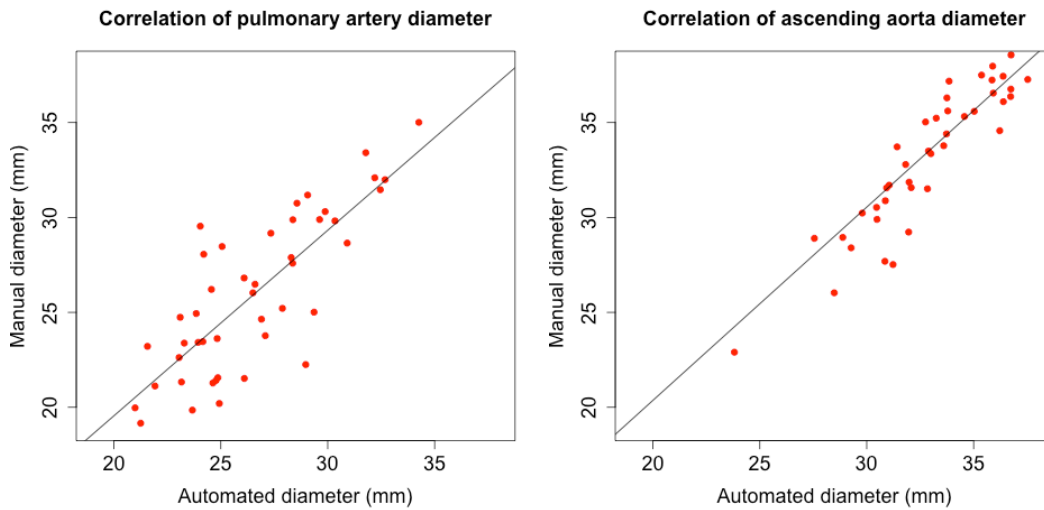

Figure 6 Correlation between automated and manual diameter measurement. Left graph shows the pulmonary artery diameter correlation and right graph shows the ascending aorta diameter correlation.
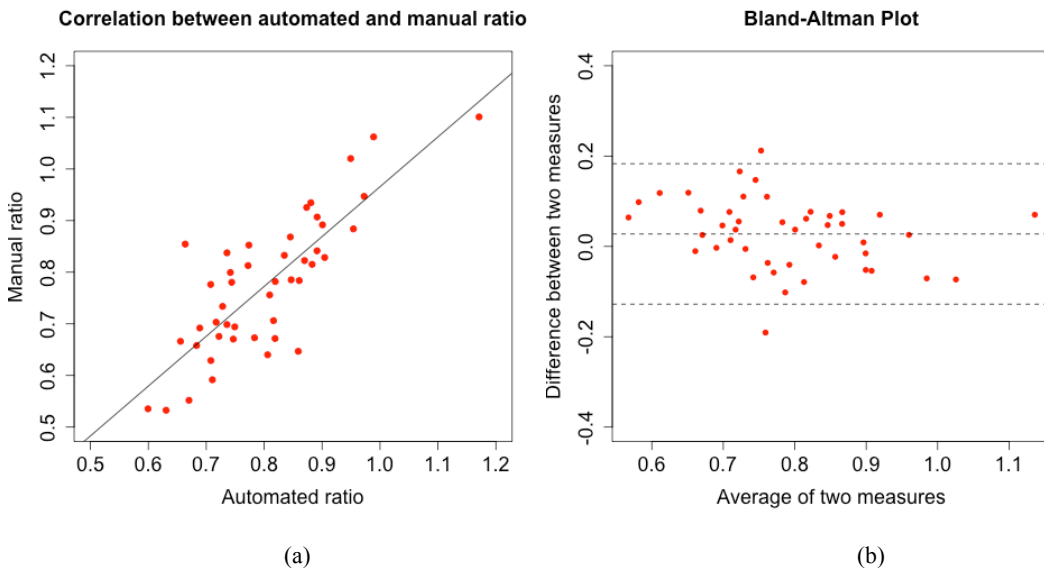

(a) (b)

Figure 7 (a) correlation between automated and manual diameter ratio; (b) Bland-Altman plot using the automated and manual ratio measurements.

5. DISCUSSION

Overall the automated segmentation had good performance with an average DSC of 0.88. Inaccurate segmentation mostly occurred in regions where: 1) the pulmonary artery was adjacent to other soft tissues such as the ascending aorta; 2) the heart motion in the un-gated CT scans caused boundary ambiguity (see Figure 5 Case3 and Case4). The pulmonary artery diameter in this study (mean diameter of 26-27mm and mean ratio of 0.77-0.80) was comparable to literature (Edwards et al[1] reported an upper limit of 33.2mm for normal pulmonary artery diameter; Karazincir et al[2] reported a mean diameter of 26.6mm and an upper limit of 32.6mm for normal diameter; Truong et al[4] reported a mean diameter of 25.1mm and a mean pulmonary artery to ascending aorta diameter ratio of 0.77; Vitanovski et al[5] reported a mean diameter of 30.2mm; Linguraru et al[6] reported a mean diameter of 33.73mm for pulmonary artery hypertension group and 25.17mm for normal group).

The automated pulmonary artery to ascending aorta diameter ratio was 0.81 correlated with the manual ratio and the Bland-Altman analysis also showed good agreement with a mean difference of 0.03 and a LOA of (-0.12, 0.18). After visually inspecting the cases with relatively larger disagreement, the following potential causes were observed:

(1) Inaccurate automated segmentation due to lack of boundary evidence (Figure 5 Case4). In these cases, the automated diameter was in general larger than the manual diameter;
(2) The two measurements were conducted at different locations (bifurcation v.s. region between bifurcation and heart). Therefore there might be a true difference in diameter.

6. CONCLUSION

The pulmonary artery in between the heart and the bifurcation has been segmented using an automated algorithm in low-dose non-contrast CT images. Using 347 low-dose and standard-dose CT scans for evaluation, the automated method had good results in 324 cases based on visual inspection. Compared to manually marked boundaries on 45 cases, the automated method had an average DSC of 0.88. The automated pulmonary artery to ascending aorta diameter ratio was 0.81 correlated with the manual ratio obtained at the bifurcation level (Bland-Altman analysis mean difference 0.03 and LOA (-0.12, 0.18)). This automated measurement of the pulmonary artery in low-dose CT images may be useful in the assessment of major artery hypertension disease risks.

ACKNOWLEDGMENTS

REFERENCES

[1] Edwards, P. D., Bull, R. K. and Coulden, R., "CT measurement of main pulmonary artery diameter," The British Journal of Radiology, 71 (850), 1018-1020 (1998).
[2] Karazincir, S., Balci, A., Seyfeli, E., Akoglu, S., Babayigit, C., Akgul, F., Yalcin, F. and Egilmez, E., "CT assessment of main pulmonary artery diameter," Diagn Interv Radiol, 14 (2), 72-74 (2008).
[3] Devaraj, A., Wells, A. U., Meister, M. G., Corte, T. J., Wort, S. J. and Hansell, D. M., "Detection of Pulmonary Hypertension with Multidetector CT and Echocardiography Alone and in Combination," Radiology, 254 (2), 609-616 (2010).
[4] Truong, Q. A., Massaro, J. M., Rogers, I. S., Mahabadi, A. A.,Kriegel, M. F., Fox, C. S., O'Donnell C. J. and Hoffmann, U., "Reference Values for Normal Pulmonary Artery Dimensions by Noncontrast Cardiac Computed Tomography: The Framingham Heart Study," Circ Cardiovasc Imaging, 5 (1), 147-154 (2012).

[5]   Vitanovski, D., Ionasec, R. I., Georgescu, B., Huber, M., Taylor, A. M., Hornegger, J. and Comaniciu, D., "Personalized Pulmonary Trunk Modeling for Intervention Planning and Valve Assessment Estimated from CT Data," MICCAI, 17-25 (2009).

[6]   Linguraru, M. G., Pura, J. A., Van Uitert, R. L., Mukherjee, N., Summers, R. M., Minniti, C., Gladwin, M. T., Kato, G., Machado, R. F. and Wood, B. J., "Segmentation and quantification of pulmonary artery for noninvasive CT assessment of sickle cell secondary pulmonary hypertension," Med. Phys, 37 (4), 1522-1532 (2010).

[7]   Xie, Y., Cham, M. D., Henschke, C., Yankelevitz, D. and Reeves, A. P., "Automated coronary artery calcification detection on low-dose chest CT images," Proc. SPIE Medical Imaging 9035, 90350F (2014).

[8]   Xie, Y., Padgett, J., Biancardi, A. M. and Reeves, A. P., "Automated aorta segmentation in low-dose chest CT images," Int J CARS, 9, 211-219 (2014).

[9]   VIA-ELCAP Public Lung Image Database, http://www.via.cornell.edu/databases/lungdb.html (18 December 2014).

[10] Armato, S. G. 3rd, McLennan, G, Bidaut, L., McNitt-Gray, M. F., Meyer, C. R., Reeves, A. P., Zhao, B., Aberle, D. R., Henschke, C. I., Hoffman, E. A., Kazerooni, E. A., MacMahon, H., Van Beeke, E. J., Yankelevitz, D., Biancardi, A. M., Bland, P. H., Brown, M. S., Engelmann, R. M., Laderach, G. E., Max, D., Pais, R. C., Qing, D. P., Roberts, R. Y., Smith, A. R., Starkey, A., Batrah, P., Caligiuri, P., Farooqi, A., Gladish, G. W., Jude, C. M., Munden, R. F., Petkovska, I., Quint, L. E., Schwartz, L. H., Sundaram, B., Dodd, L. E., Fenimore, C., Gur, D., Petrick, N., Freymann, J., Kirby, J., Hughes, B., Casteele, A. V., Gupte, S., Sallamm, M., Heath, M. D., Kuhn, M. H., Dharaiya, E., Burns, R., Fryd, D. S., Salganicoff, M., Anand, V., Shreter, U., Vastagh, S., Croft, B. Y., "The Lung Image Database Consortium (LIDC) and Image Database Resource Initiative (IDRI): A Completed Reference Database of Lung Nodules on CT Scans," Medical Physics. 38(2), 915-931 (2011).